Low-Temperature Energy Transfer in LHC-II Trimers from the Chl *a/b* Light-Harvesting Antenna of Photosystem II

Sergei Savikhin,* Herbert van Amerongen,*‡ Stefan L. S. Kwa,‡ Rienk van Grondelle,‡ and Walter S. Struve*
*Ames Laboratory-United States Department of Energy and Department of Chemistry, Iowa State University, Ames, Iowa 50011 USA, and ‡Department of Physics and Astronomy, Free University, Amsterdam, The Netherlands

ABSTRACT Temperature dependence in electronic energy transfer steps within light-harvesting antenna trimers from photosystem II was investigated by studying Chl *a* pump-probe anisotropy decays at several wavelengths from 675 to 682 nm. The anisotropy lifetime is markedly sensitive to temperature at the longest wavelengths (680–682 nm), increasing by factors of 5 to 6 as the trimers are cooled from room temperature to 13 K. The temperature dependence is muted at 677 and 675 nm. This behavior is modeled using simulations of temperature-broadened Chl *a* absorption and fluorescence spectra in spectral overlap calculations of Förster energy transfer rates. In this model, the 680 nm anisotropy decays are dominated by uphill energy transfers from 680 nm Chl *a* pigments at the red edge of the LHC-II spectrum; the 675 nm anisotropy decays reflect a statistical average of uphill and downhill energy transfers from 676-nm pigments. The measured temperature dependence is consistent with essentially uncorrelated inhomogeneous broadening of donor and acceptor Chl *a* pigments.

INTRODUCTION

The structure and energy transfer kinetics in LHC-II, the Chl *a/b* light-harvesting antenna complex associated with Photosystem II in green plants, have been studied extensively by crystallography (Kühlbrandt et al., 1983; Kühlbrandt and Downing, 1989; Kühlbrandt and Wang, 1991), by optical dichroism (Hemelrijk et al., 1992; Kwa et al., 1992a), and by ultrafast laser spectroscopy (Gillbro et al., 1985, 1988; Eads et al., 1989; Kwa et al., 1992b). This abundant, densely packed antenna (in which the chromophores comprise ~30% of the antenna-protein mass) is organized into trimers of 25 and 27 kDa apoprotein monomers that bind about 15 Chl *a* and *b* pigments (Kühlbrandt and Wang, 1991). Nearest-neighbor distances between pigments in a monomer range from 9 to 14 Å (Kühlbrandt and Wang, 1991). The Q_y absorption spectrum of LHC-II trimers contains at least 6 (and probably more) Chl spectral components (Hemelrijk et al., 1992; Kwa et al., 1992; Krawczyk et al., 1993). The CD spectrum shows evidence for strong exciton coupling between Chl *a* and *b* pigments; polarized fluorescence excitation spectra indicate that efficient energy transfer occurs among the redmost Chl *a* pigments responsible for the 676-nm component in the LHC-II spectrum.

The room temperature energy transfer dynamics of LHC-II trimers were recently studied in one- and two-color pump-probe experiments with 3–4 and 5–8 ps resolution, respectively (Kwa et al., 1992b). The one-color isotropic absorption difference profiles exhibited dynamic red-shifting with 2–6 ps kinetics, arising from downhill energy transfer among Chl spectral forms. Analyses of these profiles with triexponential decay models revealed two additional families of lifetimes: 14–36 ps (largely due to exciton annihilation), and at least several hundred picoseconds. Resolvable one-color anisotropy decays were found with lifetimes 4–6 ps at the longest Chl *a* wavelengths (665–675 nm); no discernible anisotropy decay was found at shorter wavelengths in the Chl *b* region (640–650 nm). Even at the longer wavelengths, the presence of an unresolvable (subpicosecond) anisotropy decay component was indicated by the appearance of initial anisotropies $r(0) < 0.4$. Very recently, Du et al. (1993) found 200–300 fs anisotropy components in LHC-II fluorescence upconversion experiments. Spectral evolution was studied in two-color experiments (Kwa et al., 1992b) that monitored absorption changes after Chl *b* excitation at 650 nm. While the prompt difference spectrum showed intense photobleaching/stimulated emission from the laser-excited Chl *b* pigments, it became dominated within <2.5 ps by a low energy Chl *a* difference spectrum (photobleaching/stimulated emission band maximum >675 nm). Hence, the bulk of the room-temperature spectral equilibration in LHC-II occurs with subpicosecond kinetics. This is consistent with the observation of ~500 fs Chl *b* → Chl *a* energy transfer kinetics in a fluorescence upconversion study by Eads et al. (1989). However, the slower (4–6 ps) Chl *a* → Chl *a* energy transfers reflected in the one-color anisotropy decays (Kwa et al., 1992) are reminiscent of earlier work by Gillbro et al. (1985), who characterized ~20 ps Chl *a* anisotropy decays at 665 nm. Hence, while subpicosecond spectral equilibration occurs in LHC-II trimers, slower processes are also discernible in energy transfers among their redmost Chl *a* pigments. The difference in anisotropy decay times measured by Gillbro et al. (1985) and by Kwa et al. (1992) may stem from the isolation procedures used by the respective groups; Hemelrijk et al. (1992) showed that the solubilizing

Received for publication 21 October 1993 and in final form 24 February 1994.

Address reprint requests to Walter R. Struve, Department of Chemistry, Gilman Hall, Iowa State University, Ames, IA 50011-3111. Tel.: 515-294-6342; Fax: 515-294-0105; E-mail: wstruve@ameslab.gov.

Abbreviations used: BisTris, 2-[bis(2-hydroxyethyl)amino]-2-hydroxymethylpropane-1,3-diol; CD, circular dichroism; Chl, chlorophyll; LD, linear dichroism; LHC-II, light-harvesting chlorophyll *a/b* complex II.

0006-3495/94/05/1597/07 $2.00

detergents used for isolation of LHC-II trimers can influence their LD and CD spectra.

Our principal objective in this work is to gain insight into the temperature dependence of energy transfer steps in the LHC-II antenna. In a pump-probe study of antenna Chl *a* photobleaching and stimulated emission in "native" Photosystem I particles (PSI-200) from spinach, the anisotropy decay time at 680 nm varied systematically from 63 ps at 38 K to 5 ps at 300 K (Lyle and Struve, 1991). This behavior could be simulated using a theory of Jortner (1976) for temperature dependence in energy transfer rates, by assuming that the Chl *a* Q_y transition is coupled to a $\sim 20\ cm^{-1}$ phonon mode as suggested by a spectral hole-burning study of similar PS I particles (Gillie et al., 1989). However, although the *anisotropy* decays accelerated by an order of magnitude in this temperature regime, the *isotropic* photobleaching decays (which are influenced by collective kinetics of antenna excitation transport and trapping by the P700 reaction center) showed far less temperature sensitivity. The isotropic decays clearly do not stem from sequences of energy transfer steps similar to the ones responsible for the 680 nm anisotropy decays. We report here a temperature study of one-color anisotropy decays for LHC-II at several wavelengths from 675 to 682 nm. Strong temperature dependence is observed only at the extreme red edge (680–682 nm) of the LHC-II spectrum; the anisotropy decays depend weakly on temperature at 675 nm. This behavior is rationalized using a theory for thermal broadening in Chl *a* absorption and fluorescence spectra (Rebane, 1970; Personov, 1983; Hayes et al., 1988; Gillie et al., 1989).

MATERIALS AND METHODS

LHC-II trimers were isolated from spinach thylakoids as described earlier (Hemelrijk et al., 1992; Kwa et al., 1992b). Membrane fragments were solubilized with 1% (w/v) *n*-dodecyl-β, D-maltoside in a buffer containing 20 mM BisTris, 20 mM $MgCl_2$, 10 mM $MgSO_4$, and 5 mM $CaCl_2$ at pH 6.5. LHC-II trimers in the solubilized fraction were separated from the Photosystem II core complex on a Q-Sepharose column (Kwa et al., 1992b; van Leeuwen et al., 1991). The LHC-II-rich eluate was centrifuged on a linear sucrose gradient at 4°C in a Beckman SW 41 rotor at 41,000 rpm for 16 h. The Q_y spectra of the LHC-II preparations were similar to those reported by Hemelrijk et al. (1992); samples were stored in the dark near 0°C. Pump-probe experiments were performed with samples in a buffer of 20 mM BisTris with 20 mM NaCl and 0.03% dodecylmaltoside at pH 6.5. For some room-temperature experiments, samples (which exhibited ~0.4 A at 676 nm in 0.1 cm path length cell) were translated periodically over ~2 cm at 2 Hz to minimize photodegradation. For low temperature studies, samples were placed in a window assembly (0.5 mm spacing between optical flats) in thermal contact with the end of a 2.25 cm diameter Cu cold finger in an Air Products (Allentown, PA) DE202 closed-cycle He expander module. The sample temperature, monitored directly with a calibrated Cu-constantan (Type T) thermocouple, was controllable from 13 to 300 K.

The lasers and pump-probe apparatus have been described previously (Kwa et al., 1992b). A hybrid mode-locked dye laser (DCM laser dye, DDCI saturable absorber) was pumped with 532 nm SHG pulses (70 ps fwhm, 1 W average power) from a cw mode-locked Nd:YAG laser. Typical dye laser pulses exhibited 2–3 ps fwhm autocorrelation, and were tunable from 640 to 685 nm with ~2 nm spectral bandwidth. The dye laser output was divided into pump and probe beams using an inconel-coated beamsplitter; their sample-transmitted intensities I_{pump} and I_{probe} were monitored independently using EG&G FOD-100 photodiodes for normalization of time-dependent absorption difference profiles. A radiofrequency multiple modulation scheme (Anfinrud and Struve, 1986) was employed for detection of the small absorption difference signal component ($\Delta A \sim 10^{-4}$) appearing at the sum of pump and probe beam modulation frequencies. In all experiments, absorption difference profiles $\Delta A_{\parallel}(t)$ and $\Delta A_{\perp}(t)$ were obtained with probe pulses polarized parallel and perpendicular to the pump polarization. From these, the isotropic decay function was evaluated using $\Delta A(t) = \Delta A_{\parallel}(t) + 2\Delta A_{\perp}(t)$, whereas the anisotropy decay function was computed from

$$r(t) = \frac{\Delta A_{\parallel}(t) - \Delta A_{\perp}(t)}{\Delta A(t)}. \quad (1)$$

Isotropic decays were fitted with multiexponential decay models, using a nonlinear least-squares technique based on the Simplex method. Here the instrument function $C(t)$ was represented by Gaussian fits to the apparatus autocorrelation function obtained using a $LiIO_3$ Type I SHG crystal in place of the sample. Anisotropic decays were analyzed similarly in terms of the single-exponential decay law

$$r(t) = [r(0) - r(\infty)]e^{-t/\tau} + r(\infty). \quad (2)$$

Because the anisotropic signals are related to the isotropic signal $P(t)$ in an orientationally random sample by

$$\Delta A_{\parallel}(t) = P(t)[1 + 2r(t)] \qquad \Delta A_{\perp}(t) = P(t)[1 - r(t)], \quad (3)$$

the empirical anisotropy function $r_e(t)$ is

$$r_e(t) = \frac{\int_{-\infty}^{\infty} C(t')P(t - t')r(t - t')\,dt'}{\int_{-\infty}^{\infty} C(t')P(t - t')\,dt'}. \quad (4)$$

If $P(t)$ and $r(t)$ are defined to be zero for $t < 0$, and if the isotropic decay function $P(t)$ is essentially constant on the decay time scale of $r(t)$, the empirical anisotropy function becomes

$$r_e(t) = \frac{\int_{-\infty}^{\infty} C(t')r(t - t')\,dt'}{\int_{-\infty}^{\infty} C(t')\,dt'}. \quad (5)$$

This fact was used in convolute-and-compare analyses of the measured anisotropy functions in terms of the decay model in Eq. 2.

RESULTS

Temperature dependence of energy transfer

In the earlier room-temperature study (Kwa et al., 1992b), LHC-II trimers exhibited anisotropic lifetimes of 6.3 ± 2, 5.0 ± 2, and 4.3 ± 2 ps at the pump-probe wavelengths 660, 665, and 675 nm, respectively. We have recently confirmed in room-temperature experiments (not shown) that anisotropy decay times of 5 ± 2 ps are found at all wavelengths from 665 to 685 nm. These may be contrasted with the low temperature anisotropy decays, which are exemplified for the wavelengths 675, 677, and 680 nm in Fig. 1. Reducing the temperature does not affect significantly the anisotropy decay at 675 nm (8.1 ± 2 ps at 13 K). However, the corresponding decay at 680 nm is decelerated by a factor of ~6 (from ~5 to ~30 ps lifetime) when the trimers are cooled to 13 K. Intermediate behavior is found at 677 nm (11 ± 3 ps at 13 K). Fig. 2 plots 675 and 680 nm anisotropy decay times versus temperature between 13 and 300 K: the marked temperature dependence at 680 nm is considerably diminished at 675 nm. The Boltzmann factors that govern the absorption difference spectrum after spectral equilibration tend to concentrate the excitations in the lowest-energy Chl *a* pigments and to restrict severely the wavelength range (675–682 nm)

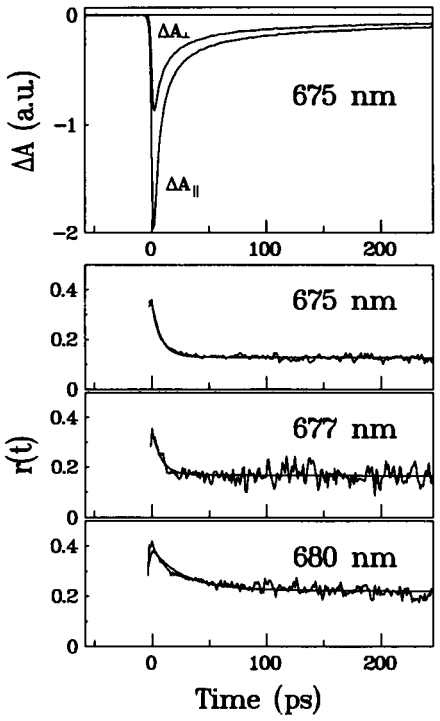

FIGURE 1 (*Top panel*) Typical anisotropic absorption difference profiles for LHC-II trimers at 675 nm and 13 K. (*Bottom* three panels) 13 K anisotropy decays $r(t)$ at 675, 677, and 680 nm. Smooth curves show optimized single-exponential fits to experimental anisotropy decays. Fitted anisotropy decay times at these wavelengths are 8, 11, and 30 ps, respectively. The (negative) absorption difference signal is dominated by photobleaching and stimulated emission. Systematic deviations between the 680 nm experimental and fitted curves show evidence for nonexponentiality in anisotropy decays.

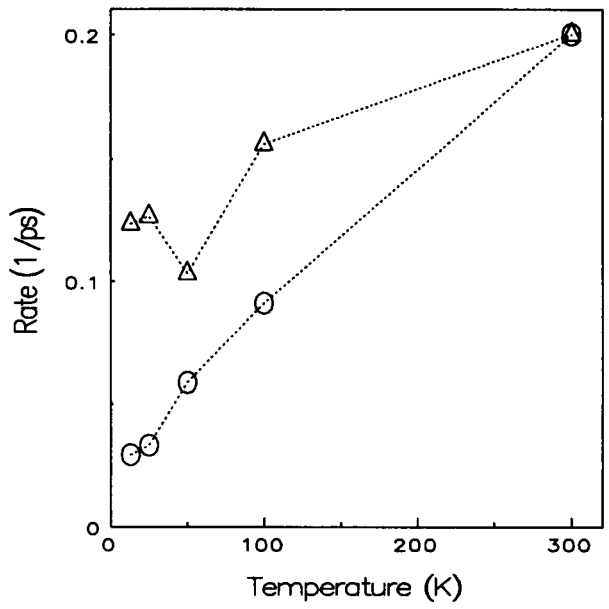

FIGURE 2 Temperature dependence of LHC-II anisotropy decay times at pump-probe wavelengths 680 nm (○) and 675 nm (△). Reciprocal decay times ($1/\tau$) are plotted rather than τ, for comparison with energy transfer simulations in Fig. 5.

over which anisotropy measurements can be made with sufficient S/N at low temperatures. Fig. 2 nevertheless documents the existence of strong wavelength inhomogeneity in the temperature dependence of energy transfer steps and suggests that marked temperature sensitivity is limited to energy transfers involving Chl *a* pigments at the extreme red edge of the LHC-II Q_y spectrum. Final parameters from single-exponential fits to several anisotropy decays are listed in Table 1 for several wavelengths at 13 and 300 K. As in the earlier pump-probe study (Kwa et al., 1992), the residual anisotropies $r(\infty)$ at 300 K are small (≤ 0.02) at most wavelengths. There is a suggestion of a trend toward larger $r(\infty)$ at the longest wavelengths ($r(\infty) = 0.05 \pm 0.01$ at 685 nm). This trend is much more pronounced at 13 K, where r(∞) increases monotonically from 0.14 ± 0.02 at 675 nm to 0.40 ± 0.03 at 685 nm. At the longest wavelength studied (685 nm), almost no depolarization is detected. The enhanced residual polarization at longer wavelengths parallels a similar wavelength trend observed in the fluorescence polarization of LHC-II trimers (Hemelrijk et al., 1992). Table 2 documents the temperature dependence in the 680 nm anisotropy decay parameters between 13 and 300 K. Although cooling increases the anisotropy decay time at this wavelength from 5 to 34 ps, the residual anisotropy concomitantly increases from 0.03 ± 0.01 to 0.19 ± 0.02.

TABLE 1 Wavelength dependence of anisotropy decay parameters

$$r(t) = [r(0) - r(\infty)]e^{-t/\tau} + r(\infty)$$

T = 13 K				T = 300 K			
λ	$r(0)$	$r(\infty)$	τ	λ	$r(0)$	$r(\infty)$	τ
nm			ps	nm			ps
675	0.34	0.14	8.1	665	0.32	0.02	5
677	0.36	0.17	7.3	670	0.32	0.00	5
	0.35	0.17	11	675	0.32	0.02	5
	0.33	0.16	11	680	0.33	0.03	5
	0.35	0.17	14	685	0.34	0.05	5
680	0.36	0.20	38				
	0.34	0.20	30				
	0.32	0.19	34				
682	0.36	0.26	29				
685	0.40	0.40	—				

The corresponding isotropic decays $\Delta A(t)$ are relatively insensitive to temperature, even at 680 nm. This contrast in behavior between isotropic and anisotropic decays underscores the nonuniformity of temperature dependence for energy transfers in this antenna.

DISCUSSION

We first consider the mechanism(s) by which Chl *a* energy transfer kinetics monitored through 680 nm anisotropy decays can accelerate by a factor of 5–6 when the temperature is raised from 13 to 300 K (Fig. 2). In the context of Förster theory for dipole-dipole energy transfer, such thermal effects originate from temperature-dependent changes in the overlap

TABLE 2 Temperature dependence of anisotropy decay parameters at 680 nm

$r(t) = [r(0) - r(\infty)]e^{-t/\tau} + r(\infty)$

T	$r(0)$	$r(\infty)$	τ
K			ps
13	0.32	0.19	34
25	0.33	0.16	30
50	0.33	0.13	17
100	0.33	0.09	11
300	0.33	0.03	5

integral (Dexter, 1953)

$$\int d\omega f_D(\omega)\sigma_A(\omega)/\omega^4$$

between the normalized donor fluorescence spectrum and the acceptor absorption cross section. Thus, temperature modeling of Förster rates focuses on simulating the temperature dependence of pigment absorption and fluorescence spectra (Jia et al., 1992). This stems from electron-phonon and electron-vibration interactions, which lead to differences between the nuclear mode frequencies and equilibrium geometries in the pigments' electronic ground and Q_y states. When the ground and excited state vibrational Hamiltonians are given by

$$H_g = \frac{-\hbar^2\partial^2}{2\mu\partial Q^2} + \frac{1}{2}\mu\omega_s^2 Q^2$$
$$H_e = \frac{-\hbar^2\partial^2}{2\mu\partial Q^2} + \frac{1}{2}\mu(\omega_s')^2(Q - \Delta)^2, \quad (6)$$

the strength of the electron-nuclear coupling can be characterized by the dimensionless Huang-Rhys parameter

$$S = \frac{\mu\omega_s\Delta^2}{2\hbar}. \quad (7)$$

In a spectral hole-burning study of the antenna Chl *a* Q_y spectrum in photosystem I particles from spinach, Gillie et al. (1989) determined the frequencies, Huang-Rhys factors, and (in some cases) frequency shifts for 41 Chl *a* vibrational modes. These intramolecular modes (whose frequencies are distributed from 262 to 1524 cm^{-1}) exhibit small S ($\leq$0.044) and small fractional frequency shifts ($\leq$3%). The temperature dependence of the Chl *a* absorption spectrum in PS I is dominated by a highly Franck-Condon active 22 cm^{-1} phonon mode (S = 0.8). In LHC-II, the Chl *a* intramolecular vibrations must exhibit similar parameters, but the Franck-Condon active 20 cm^{-1} phonon exhibits a Huang-Rhys factor of ~0.3 to 0.4 at 4 K (N. R. Reddy and G. J. Small, unpublished data). The low temperature, single-site absorption profile for a Franck-Condon active phonon with frequency ω_s and Huang-Rhys factor S may be written as (Personov, 1983; Hayes et al., 1988)

$$\alpha_p(\omega) = e^{-S}l_0(\omega) + \sum_{r=1}^{\infty}\frac{S^r e^{-S}}{r!}l_r(\omega - r\omega_s). \quad (8)$$

Here the values of r correspond to zero-, one-, etc. phonon transitions. The r-phonon profile $l_r(\omega)$ is obtained by convoluting the one-phonon profile $l_1(\omega)$ with itself ($r - 1$) times; $S^r\exp(-S)/r!$ is the Franck-Condon factor for the r-phonon band, which is centered at frequency $r\omega_s$. Incorporating N vibrational modes with frequencies δ_ν and Huang-Rhys factors S_ν converts the low temperature, single-site profile into a superimposition of phonon profiles centered at the t-vibration transition frequencies $t\omega_\nu$ and weighted by Franck-Condon factors,

$$\alpha(\omega) = \sum_{\nu=1}^{N}\sum_{t=0}^{\infty}\frac{S_\nu^t e^{-S_\nu}}{t!}\alpha_p(\omega - t\omega_\nu). \quad (9)$$

For realism, site distributions in the vibrational frequencies may be included through the incorporation of t-vibration profiles $m_t(\omega)$ that are analogous to the r-phonon profiles $l_r(\omega)$. Inhomogeneous broadening in the 0–0 electronic transition frequency must also be taken into account. Extension of this theory to finite temperatures allows for inclusion of hot absorption bands; the Huang-Rhys factors S are superseded everywhere (Rebane, 1970) by a temperature-dependent parameter $S(T) = S(0)\coth(\hbar\omega/2kT)$. In these simulations, the Chl *a* absorption spectra are little affected by the choice of zero-phonon and zero-vibration profiles $l_0(\omega)$ and $m_0(\omega)$ if their widths are small compared to inhomogeneous broadening in the Q_y energies. The zero-phonon and zero-vibration profiles were modeled with Lorentzian and Gaussian profiles, respectively, with 1 cm^{-1} fwhm. The spectra are far more sensitive to site inhomogeneity in the electronic transition frequency, which was represented by Gaussian distributions with 10, 50, 100, or 150 cm^{-1} fwhm. Spectral hole-burning studies indicate that the Gaussian spectral width for electronic site inhomogeneity in the Chl *a* absorption spectrum is ~200 cm^{-1} (Hayes et al., 1988). More recent experiments on LHC-II trimers indicate that Chl *a* pigments in this antenna typically exhibit inhomogeneous broadening of 100–120 cm^{-1} (Kwa et al., 1992a; Krawczyk et al., 1993; N. R. Reddy and G. J. Small, unpublished data). In our calculations, each fluorescence spectrum was approximated as the mirror image of the absorption spectrum at that temperature; this is valid if the vibrational frequency shifts ($\omega_s' - \omega_s$) are small (Jia et al., 1992).

The practice of using Chl *a* absorption profiles with inhomogeneous broadening parameters drawn from analyses of empirical absorption spectra is a serious approximation in two respects. First, the energy transfer kinetics observed between two chromophores in the presence of inhomogeneous broadening will be nonexponential, because the rate constants depend (*inter alia*) on the donor-acceptor energy gaps. The anisotropy decays in Fig. 1, for example, exhibit indications of nonexponentiality. Hence, it would be more correct to calculate theoretical rate constants for all possible combinations of donor and acceptor site energies, and then to weight the kinetics over the inhomogeneously broadened profiles. Using inhomogeneously broadened profiles directly in the spectral overlap integral has the effect of representing

the true multiphasic energy transfer kinetics with a single, averaged rate constant. In this work, the limited S/N in our anisotropy decays does not warrant fitting them with multiexpoential model functions; instead, experimental lifetimes from single-exponential fits are compared with effective rate constants computed from spectral overlap between inhomogeneously broadened profiles. Second, the appropriateness of using Gaussian widths from absorption spectra in simulations of the spectral overlap depends on whether correlations exist between donor and acceptor site inhomogeneities (Jia et al., 1992). The presence of such correlations would reduce the effective site inhomogeneity in the spectral overlap integral.

Fig. 3 displays model absorption and fluorescence spectra for Chl *a* acceptor and donor pigments with a 0–0 Q_y energy gap of +200 cm^{-1} (i.e., uphill energy transfer). The Gaussian broadening (50 cm^{-1} fwhm) and temperatures (10 and 300 K) were chosen here to illustrate extreme temperature dependence in spectral overlap. Under these conditions, the Förster rate constants evaluated at 10 and 300 K differ by a factor of ~60. Larger inhomogeneous broadening and/or smaller energy gaps blunt this temperature sensitivity. In Fig. 4, we show the simulated temperature dependence of up- and downhill energy transfer rates for 150, 100, 50, and 10 cm^{-1} inhomogeneous broadening, for a range of donor-acceptor energy gaps. This figure illustrates several trends.

(a) For *isoenergetic* transfers (zero donor-acceptor energy gap), the effective rate constant *decreases* when the temperature is raised. This stems from the fact that most of the spectral overlap in the case of zero energy gap occurs between the intense 0–0 acceptor absorption and donor fluorescence bands (cf. Fig. 3). This overlap (which is large for isoenergetic transfers at low T) becomes reduced at higher T, because the absorption and fluorescence bands become asymmetrically broadened in opposite directions when the temperature is raised.

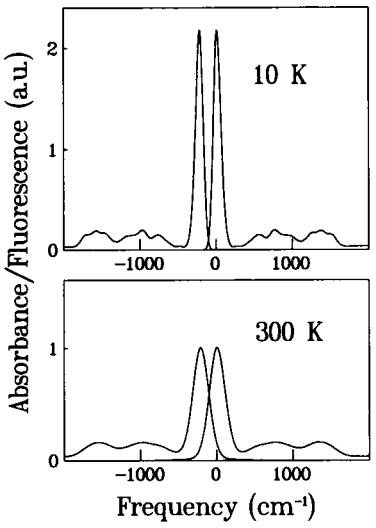

FIGURE 3 Simulated fluorescence and absorption spectra at 10 K (*top*) and 300 K (*bottom*) for Chl *a* donor and acceptor species with 200 cm^{-1} Q_y energy gap. Inhomogeneous Gaussian broadening is 50 cm^{-1} fwhm; Huang-Rhys factor $S(0)$ for the Franck-Condon active phonon mode is 0.8.

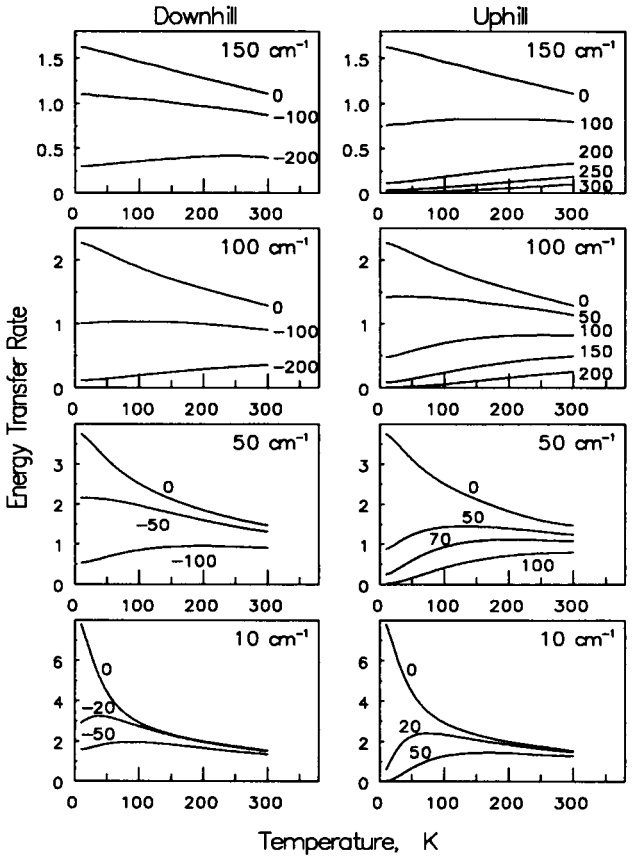

FIGURE 4 Simulated temperature dependence of uphill and downhill energy transfer rates for Chl *a* donor and acceptor species with inhomogeneous broadening of (from top) 150, 100, 50, and 10 cm^{-1}. Huang-Rhys factor $S(0)$ for the Franck-Condon active phonon mode is 0.35. Large numbers indicate Gaussian fwhm of inhomogeneous broadening profile in cm^{-1}; small numbers indicate Q_y energy gaps in cm^{-1}. Energy transfer rates are in arbitrary units, but are mutually normalized for all conditions in this figure.

(b) The temperature dependence of *downhill* energy transfer kinetics (where the energy gap is comparable to or larger than the inhomogeneous broadening) is comparatively weak. This arises because much of the spectral overlap in this case occurs between the 0–0 donor fluorescence band and the broad quasicontinuum of higher vibronic bands in the acceptor absorption spectrum, and vice versa.

(c) Significant temperature dependence occurs in *uphill* energy transfers, where increased temperatures are accompanied by larger spectral overlaps between the donor and acceptor 0–0 bands (cf. Fig. 3). In this case, the Chl *a* higher vibronic bands contribute negligibly to the spectral overlap. Because downhill energy transfers do not lead to reductions by factors as large as ~6 in the transfer rate (Fig. 4), the temperature dependence observed in the 680-nm anisotropies appears to be consistent only with uphill energy transfer.

For 10 and 50 cm^{-1} inhomogeneous broadening, most of the temperature variations in the uphill energy transfer kinetics occur at temperatures below 100 K, in contrast to the

anisotropy decays observed at 680 nm (Fig. 2 and Table 2). Hence, the energy transfers observed at this wavelength appear to be dominated by uphill processes between pigments with an effective inhomogeneous broadening of at least $\sim$100 cm^{-1}. For such inhomogeneous broadening, our calculations (Fig. 4) indicate that the donor-acceptor energy gap must be on the order of 100–150 cm^{-1} to produce a ratio of 6:1 for the average energy transfer rates at 300 and 13 K. Because the inhomogeneous broadening required to simulate the temperature dependence at 680 nm is comparable to the 100–120 cm^{-1} inhomogeneous broadening observed in LHC-II absorption spectra (Krawczyk et al., 1993; Reddy and Small, unpublished results), these experiments suggest that the donor and acceptor site inhomogeneities are essentially uncorrelated for these energy transfers.

If the donor pigments in the temperature-dependent energy transfer steps are the same as the ones directly excited by the laser, the operative donor inhomogeneous broadening cannot be larger than the laser excitation bandwidth of 2–3 nm ($\sim$50 cm^{-1}). Hence, the calculations performed under the assumption of 100 and 150 cm^{-1} inhomogeneous broadening were repeated for 50 cm^{-1} donor inhomogeneous broadening, combined with 100 or 150 cm^{-1} acceptor inhomogeneous broadening. The results were similar to those in Fig. 4, except that slightly smaller uphill energy gaps ($\sim$120 vs. 150 cm^{-1}, in the case of 100 cm^{-1} acceptor inhomogeneous broadening) were required to simulate the experimental temperature dependence.

The Q_y electronic level structure of LHC-II trimers is not yet well understood. The identities (*a* versus *b*) and transition moment orientations of the Chl pigments characterized by Kühlbrandt and Wang (1991) have not been assigned. No model exciton calculations have been attempted with the purpose of simulating their electronic spectra. The lowest-energy Chl *a* spectral form discernible in static absorption, LD, and CD spectra of similar LHC-II preparations exhibits a 0–0 band maximum at $\sim$676 nm (Hemelrijk et al., 1992). The relative intensity of this absorption band suggests that (in the absence of substantial intensity redistribution by resonance couplings) it stems from $\sim$12 Chl *a* pigments/trimer. Hence, one possible interpretation of the low energy Q_y spectrum is that it arises from 12 exciton levels, all with mean transition wavelength near 676 nm. In this model (hereafter called Model 1), each level is subject to random, inhomogeneous broadening (uncorrelated with that in the other low energy Chl *a* levels) on the order of 120 cm^{-1} fwhm. Under these circumstances, statistically $\sim$25% of all LHC-II trimers would contain Chl *a* pigments absorbing at $\geq$680 nm. However, spectral hole-burning studies of LHC-II trimers have suggested recently the existence of a weak Chl *a* spectral component at $\sim$680 nm (Reddy and Small, unpublished data). The low intensity of this component (<3 pigments/trimer) may be due to redistribution through exciton couplings. Similarly, our absorption difference spectra of LHC-II trimers at 13 K (not shown) exhibit a sharp photobleaching/stimulated emission maximum at $\sim$680 nm. Hence, another possible model (Model 2) visualizes that the redmost portion of the LHC-II spectrum comprises a well defined exciton level with mean transition wavelength 680 nm, in addition to a (group of) exciton level(s) with mean transition wavelength 676 nm. In the simplest version of this model, the 680- and 676-nm levels exhibit uncorrelated inhomogeneous broadening on the order of 120 cm^{-1} fwhm.

In either model, the uphill energy transfers observed in the 680 nm anisotropy decays may involve donor and acceptor Chl *a* pigments absorbing at 680 and 676 nm, respectively. For such processes, the mean energy gap would be on the order of +100 cm^{-1}. The overall 680 nm anisotropy decay may actually be dominated by a two-step process, in which energy transfer from a 680- to a 676-nm pigment is followed by a subsequent transfer to a second 680-nm species, whose orientation contrasts with that of the original 680-nm pigment. The kinetics of the latter step may be markedly faster than those of the original 680 $\rightarrow$ 676 nm energy transfer, in consequence of detailed balancing or proximity effects. The occurrence of significant energy transfers among 680-nm pigments via higher energy pigments would imply that all of the 680 nm pigments are not grouped together in one cluster. The weaker temperature dependence of the 675 nm anisotropy decays likely arises from averaging of nearly isoenergetic (676 $\rightarrow$ 676 nm), uphill, and downhill energy transfers. Finally, because 676-nm pigments are more numerous than 680-nm pigments, the overall 680 nm depolarization process may stem from multistep 680 $\rightarrow$ 676 $\rightarrow$ 676 $\rightarrow \cdots$ $\rightarrow$ 680-nm processes, with the result that the observed temperature dependence depends on the relative magnitudes of rate constants for several individual transfers. More structural information (e.g., locations and orientations of specific pigments) is required to assess the likelihood of such a scenario. However, it appears clear that isoenergetic 676 $\rightarrow$ 676 nm energy transfers do not dominate the overall temperature dependence, because the rate constants for zero donor-acceptor energy gap exhibit temperature trends that are opposite to the observed behavior (Fig. 4). Finally, a two-step process may not be necessary to explain the anisotropy behavior. Since the inhomogeneously broadened exciton components in Model 2 must overlap considerably, the 680 nm, one-color experiment will be influenced by uphill equilibration between the 680-nm state and the 676-nm state (which also absorbs at 680 nm).

The absence of significant anisotropy decay at 685 nm and 13 K ($r(\infty) \sim 0.4$, Table 1) is consistent with the observation in hole-burning of uncoupled long-wavelength Chl *a* pigments. The systematic increase in the low temperature residual anisotropy with wavelength (Table 1) may then reflect the relative contribution of uncoupled pigments to the absorption difference signal at different wavelengths. However, this scenario alone cannot explain the temperature trend in $r(\infty)$ at 680 nm (Table 2), because the fraction of uncoupled pigments should be essentially independent of temperature. The empirical energy transfer kinetics between donor and acceptor pigments with appreciable site inhomogeneity will not be monophasic (Pullerits and Freiberg, 1992), and nonexponentiality is apparent in some of the

anisotropic decays in Fig. 1. The residual anisotropy trend may then stem from components whose lifetimes are finite at room temperature, but become infinite with respect to the 250 ps time window (Fig. 1) at low temperature. In Model 1, such components can stem from energy transfer between donor pigments at the extreme red edge and acceptor pigments at the extreme blue edge of an inhomogeneously broadened 676-nm band. In Model 2, they can arise from donor pigments at the red edge of the 680-nm band and acceptor pigments at the blue edge of the 676-nm band. In Model 2, the effective uphill energy gap for such transfers can be on the order of 100 cm^{-1} larger than for pigments absorbing near the centers of the respective component bands. This possibility illustrates a caveat that must be attached to the single-exponential data analysis and simulations in the present work. The present temperature trend in residual anisotropies parallels a similar observation in the polarized fluorescence of LHC-II trimers (Hemelrijk et al., 1992), which showed that an increased fraction of the excitations becomes effectively trapped in the lowest energy pigments when the trimers are cooled.

In conclusion, marked temperature dependence is observed between 13 K and room temperature in LHC-II antenna energy transfers only at the longest pump-probe wavelengths (680–682 nm); weaker temperature dependence is observed at shorter wavelengths. This behavior can be modeled in spectral overlap simulations of energy transfer rates, based on a Förster mechanism using physically reasonable parameters for the Huang-Rhys factors, the donor-acceptor energy gap, and the inhomogeneous broadening. Our simulations of the observed temperature dependence suggest that the spectral inhomogeneity in the Chl *a* portion of the LHC-II spectrum is locally random.

Note added in proof—W. Kühlbrandt, D. N. Wang, and Y. Fujiyoshi (1994) have recently published an LHC-II structure in which the identities of Chl *a* and Chl *b* have been tentatively assigned (*Nature.* 367:614–621).

We are indebted to Dr. Tonu Pullerits for helpful discussions, and for the algorithm and computer program used in the temperature simulations of the Chl *a* absorption spectra. We also thank Professors Gerald Small and John Jean for helpful discussions. The Ames Laboratory is operated for the U.S. Department of Energy by Iowa State University under Contract No. W-7405-Eng-82.

This work was supported by the Division of Chemical Sciences, Office of Basic Energy Sciences. This research was supported in part by the Dutch Foundations for Chemical Research (SON) and for Biophysics (S.v.B), and was financed by the Netherlands Organization for Scientific Research (NWO).

REFERENCES

Allen, J. F. 1992. How does protein phosphorylation regulate photosynthesis? *Trends Biochem. Sci.* 17:12–17.

Anfinrud, P. A., and W. S. Struve. 1986. Optical shot-noise-limited detection: a single-sideband technique with flexible modulation frequencies. *Rev. Sci. Instrum.* 57:380–383.

Dexter, D. L. 1953. A theory of sensitized luminescence in solids. *J. Chem. Phys.* 21:836–850.

Du, M., X. Xie, L. Mets, and G. R. Fleming. 1993. Direct observation of the ultrafast energy transfer step in light harvesting complex II. *Photochem. Photobiol.* 57:17*a* (Abstr.)

Eads, D. D., E. W. Castner, R. S. Alberte, L. Mets, and G. R. Fleming. 1989. Direct observation of energy transfer in a photosynthetic membrane: chlorophyll b to chlorophyll a transfer in LHC. *J. Phys. Chem.* 93:8271–8275.

Gillbro, T., V. Sundström, Å. Sandström, M. Spangfort, and B. Andersson. 1985. Energy transfer within the isolated light-harvesting chlorophyll a/b protein of photosystem II (LHC-II). *FEBS Lett.* 193:267–270.

Gillbro, T., Å. Sandström, M. Spangfort, V. Sundström, and R. van Grondelle. 1988. Excitation energy annihilation in aggregates of chlorophyll a/b complexes. *Biochim. Biophys. Acta.* 934:369–374.

Gillie, J. K., G. J. Small, and J. H. Golbeck. 1989. Nonphotochemical hole-burning of the native antenna complex of Photosystem I (PSI-200). *J. Phys. Chem.* 93:1620–1627.

Hayes, J. M., J. K. Gillie, D. Tang, and G. J. Small. 1988. Theory for spectral hole burning of the primary electron donor state of photosynthetic reaction centers. *Biochim. Biophys. Acta.* 851:75–85.

Hemelrijk, P. W., S. L. S. Kwa, R. van Grondelle, and J. P. Dekker. 1992. Spectroscopic properties of LHC-II, the main light-harvesting chlorophyll a/b protein complex from chloroplast membranes. *Biochim. Biophys. Acta.* 1098:159–166.

Jia, Y., J. M. Jean, M. M. Werst, C.-K. Chan, and G. R. Fleming. 1992. Simulations of the temperature dependence of energy transfer in the PS I core antenna. *Biophys. J.* 63:259–273.

Jortner, J. 1976. Temperature-dependent activation energy for electron transfer between biological molecules. *J. Chem. Phys.* 64:4860–4867.

Krawczyk, S., Z. Krupa, and W. Maksymiec. 1993. Stark spectra of chlorophylls and carotenoids in antenna pigment-proteins LHC-II and CP-II. *Biochim. Biophys. Acta.* 1143:273–281.

Kühlbrandt, W., T. Thaler, and E. Wehrli. 1983. The structure of membrane crystals of the light-harvesting chlorophyll a/b protein complex. *J. Cell Biol.* 96:1414–1424.

Kühlbrandt, W., and K. H. Downing. 1989. Two-dimensional structure of plant light-harvesting complex at 37 Å resolution by electron crystallography. *J. Mol. Biol.* 207:823–828.

Kühlbrandt, W., and D. N. Wang. 1991. Three-dimensional structure of plant light-harvesting complex determined by electron crystallography. *Nature.* 350:130–134.

Kwa, S. L. S., F. G. Groeneveld, J. P. Dekker, R. van Grondelle, H. van Amerongen, S. Lin, and W. S. Struve. 1992a. Steady-state and time-resolved polarized light spectroscopy of the green plant light-harvesting complex II. *Biochim. Biophys. Acta.* 1101:143–146.

Kwa, S. L. S., H. van Amerongen, S. Lin, J. P. Dekker, R. van Grondelle, and W. S. Struve. 1992b. Ultrafast energy transfer in LHC-II trimers from the Chl a/b light-harvesting antenna of Photosystem II. *Biochim. Biophys. Acta.* 1102:202–212.

Larsson, U. K., C. Sundby, and B. Andersson. 1987. Characterization of two different subpopulations of spinach light-harvesting chlorophyll a/b protein complex (LHC II): polypeptide composition, phosphorylation pattern and association with photosystem II. *Biochim. Biophys. Acta.* 894:59–68.

Lyle, P. A., and W. S. Struve. 1991. Temperature dependence of antenna excitation transport in native Photosystem I particles. *J. Phys. Chem.* 95:4152–4158.

Personov, R. I. 1983. Site selection spectroscopy of complex molecules in solutions and its applications. *In* Spectroscopy and Excitation Dynamics of Condensed Molecular Systems. Vol. 4. V. M. Agranovich and R. M. Hochstrasser, editors. North-Holland, Amsterdam.

Rebane, K. K. 1970. Impurity Spectra of Solids. Plenum Press, New York.

Savikhin, S., T. Wells, P.-S. Song, and W. S. Struve. 1993. Ultrafast pump-probe spectroscopy of native etiolated oat phytochrome. *Biochemistry.* 32:7512–7518.

Van Leeuwen, P. J., M. C. Nieveen, E. J. van de Meent, J. P. Dekker, and H. J. van Gorkom. 1991. Rapid and simple isolation of pure Photosystem II core and reaction center particles from spinach. *Photosynth. Res.* 28: 149–153.